Volume 1 | Number 1 | Jan 2013 | Pages 1–100

Catalysis Science & Technology

www.rsc.org/catalysis

ROYAL SOCIETY OF CHEMISTRY

www.rsc.org/catalysis

Catalysis Science & Technology

PAPER

Gold nanoparticles supported on Ce-Zr oxides for the oxidative esterification of aldehydes to esters

Yuchao Li,[a,b] Lei Wang,[a] Ruiyi Yan,[a] Junxing Han[a] and Suojiang Zhang*[a]

Au nanoparticles supported on Ce-Zr oxides catalysts were prepared and characterized in order to study the role of support for the oxidative esterification of aldehydes in the presence of molecular oxygen. Ce-Zr solid solutions were synthesized by using $(NH_4)_2Ce(NO_3)_6$ as precursor, while the mixed oxides were obtained by $Ce(NO_3)_3$ precursor. The solid solutions exhibited smaller crystallite size, higher BET surface

10 area, and larger amount of H_2 consumption, acidity and basicity than the mixed oxides at the same Ce/Zr mole ratio due to the incorporation of Zr^{4+} into ceria lattice. The effect of the support was investigated owing to all samples presenting the similar Au particle size confirmed by HAADF-STEM study. Supports with higher reducibility showed better performances by activation of methanol to methoxy and facilitating the β-H elimination of hemiacetal. We also found that the formation of hemiacetal was enhanced by

15 acidic sites and basic sites of Au catalysts supported on solid solutions possessing similar reducibility. Plausible reaction mechanism for oxidative esterification of aldehydes on Ce-Zr solid solution supported Au nanoparticles was proposed. The screening catalyst was also applicable to the oxidative esterification of different benzyl aldehydes with high yields. The catalyst could be reused after a simple separation for eight times keeping high selectivity above 99%.

20 1.   Introduction

Esterification, one of the most fundamental reactions in organic synthesis, is extensively used in laboratories and industries.[1, 2] Contrary to the traditional two-step esterification procedure that includes the synthesis of carboxylic acids or activated carboxylic

25 acid derivatives, such as acid anhydrides or acid chlorides,[3, 4] the direct oxidative esterification of aldehydes with alcohols has great economic and environmental benefits in the synthesis of esters. Although several facile and selective esterification methods have been developed, the direct oxidative esterification

30 of aldehydes with alcohols using the ultimate oxidation agent, namely, molecular oxygen, by heterogeneous catalysts under mild conditions is an attractive topic for both organic synthesis and green chemistry.[5,6]

Since Haruta et al.[7] reported the aerobic oxidation of carbon

35 monoxide using highly dispersed Au nanoparticles supported on reducible and active supports have drawn much attention because of their high activity in aerobic oxidation reactions. In particular, several solid catalysts based on transition metal oxide-supported Au nanoparticles for oxidative esterification of aldehydes have

40 recently been reported.[6, 8-11] The performance of the Au nanoparticle-supported metal oxides depends on various factors covering the size and shape of the Au nanoparticles, the electronic state and preparation procedures.[12-16] In addition, the support also plays an important role in the dispersion of the Au

45 particles and activation of reactants,[17-21] such as O_2.

In the recent years, Ce-Zr mixed oxides have been widely used as supports for Au in many oxidation reactions.[22-24] Ce-Zr mixed oxides were selected because of their unique redox properties and high capacity of lattice oxygen, and these properties strongly

50 depend on the Ce/Zr molar ratio. In addition to these properties, Ce-Zr materials present remarkable acid–base properties, which have not been extensively investigated. The acid-base nature of the supports has a great impact on the performance of the oxidation esterification of aldehydes, according to the literature.[8,

55 11] To date, Au supported on Ce-Zr mixed oxides for oxidative esterification of aldehydes have not been reported.

This paper reports the relation between the physic-chemical properties of the Ce-Zr mixed oxides and the catalytic performance of $Au/Ce_{1-x}Zr_xO_2$ in the oxidative esterification of

60 aldehydes with methanol. $Au/Ce_{1-x}Zr_xO_2$ (x = 0, 0.2, 0.4, 0.6, 0.8, 1) oxides and $Au/Ce_{1-x}Zr_xO_2$ catalysts were prepared, characterized, and tested in aerobic oxidative esterification of aldehydes. The effect of the physic-chemical of the support has been examined according to their influence on the oxidation

65 esterification reaction. The substrate scope and the cycle times of the screening catalyst have also been investigated.

2.   Experimental

2.1. Catalyst preparation

A series of Ce-Zr mixed oxides, CeO_2 and ZrO_2 were prepared via the hydrothermal method. All supports were designed to obtain $Ce_{1-x}Zr_xO_2$ solid solution, where x was the atomic ratio of Zr/(Ce+Zr) and varied at 0, 0.2, 0.4, 0.8, and 1.0. Two Ce precursors, $Ce(NO_3)_3$ and $(NH_4)_2Ce(NO_3)_6$, were used to synthesize the Ce-Zr mixed oxides according to previously reported methods[25,26] with slight modification. The oxides are referred to as A-$Ce_{1-x}Zr_xO_2$ ($Ce(NO_3)_3$ as precursor) and B-$Ce_{1-x}Zr_xO_2$ ($(NH_4)_2Ce(NO_3)_6$ as precursor) respectively.

The typical preparation procedure was described below. Ce precursor (>99.0%, AR, Sinopharm Chemical Reagent Co. Ltd), $ZrOCl_2$ (AR, Beijing Chem. Corp.) and urea (>99.0%, AR, Beijing Chem. Corp.) in the molar ratio of Ce^{m+}: ZrO^{2+}: urea = (1–x): x : 10 (x = 0, 0.2, 0.4, 0.6, 0.8 and 1.0) were dissolved in 80 mL of deionized water in a Teflon-lined stainless steel autoclave (inner volume: 100 mL). The total cation concentration at 0.1 mol·L^{-1} was maintained. The autoclave was tightly sealed and placed in an oven for hydrothermal treatment at 413 K for 24 h. The white and yellow precipitate was obtained respectively, and then it was centrifugally separated, washed several times with deionized water, and subsequently dried at 353 K in air overnight. The as-prepared $Ce_{1-x}Zr_xO_2$ oxides were calcined in still air at 773 K for 4 h and yellow powders were obtained.

The Au nanoparticles were deposited on metal oxides by deposition–precipitation method. The pH level of an aqueous solution of $HAuCl_4$ (10^{-4} mol·L^{-1}) was adjusted to pH 10 by adding saturated Na_2CO_3 solution. Then, the solution was mixed with corresponding support to fix the Au-supported 1.5% and the pH value was maintained at 10 by saturated Na_2CO_3 solution. After stirring at 313 K for 3 h, the suspension was filtered and washed with an excess amount of deionized water until no more chlorine remained. The supported Au catalyst was dried in a vacuum oven at 313 K overnight and then calcined at 250 °C for 4 h in air.

2.2. Catalyst characterization

Transmission electron microscopy (TEM) and scanning transmission electron microscopy (STEM) measurements were performed using JEOL TEM 2011 operated at 200 kV. Samples were deposited on the TEM grids after ultrasonic dispersion in ethanol. Scanning electron microscopy (SEM) measurements were performed by S-4700 microscope (Hitachi, Japan) using a 20 kV acceleration voltage.

X-ray diffraction (XRD) measurements of the catalysts were performed on a Rigaku RINT 2500 diffractometer using monochromated Cu Kα radiation with a scan speed of 15° min^{-1} and a scan range of 20–80° at 30 kV and 15 mA.

Nitrogen adsorption/desorption isotherms at 77 K were measured using Sorptomatic 1900 apparatus (Carlo-Erba). Prior to the measurement, all samples were degassed for 4 h at 573 K. The specific surface area, S_{BET} was calculated using BET equation.

The Au lading was determined by inductive couple plasma optical emission spectrometer (ICP-OES) by IRIS Intrepid II XSP (Thermofisher, USA).

Hydrogen temperature programmed reduction (H_2-TPR) was conducted on Autochem II 2920 (Micromeritics, USA). A total of 50 mg catalyst was filled in a quartz reactor. The catalyst powders were pretreated under Ar flow (20 mL/min) at 200 ℃

for 2 h. Then the sample was cooled to 50 °C, and subsequently the test was performed with a 10% H_2/Ar gas mixture (20 mL/min) from room temperature to 900 °C (20 °C /min). The temperature-programmed desorption of ammonia and carbon dioxide (NH_3- and CO_2-TPD) experiments were carried out on Autochem II 2920 (Micromeritics, USA). The samples were pretreated under He flow (20 mL/min) at 200 °C for 2 h. The sample was cooled to 50 °C, and then exposed to 10% NH_3/He mixture or 10% CO_2/He mixture flow (20 mL/min) for 1 h. Then, the sample was flushed under He flow at 50 °C to remove physically adsorbed CO_2 or NH_3. A CO_2-TPD (or NH_3-TPD) profile of the sample was recorded by increasing the temperature from 50 °C to 800 °C at a heating rate of 10 °C/min under 20 mL/min of He flow.

2.3. Catalytic reaction

The oxidative esterification of isobutyraldehyde and other aldehydes with methanol to methyl esters was performed in a 50 mL steel autoclave. The substrate (50 mmol) and methanol (40 mL) were added into the reactor pre-charged with catalyst (typically, 0.50 g) and K_2CO_3 (typically, 0.10 g). After O_2 charge with 0.3 MPa pressure, the mixture was heated to 343 K reaction temperature, and then the catalytic reaction was started by vigorous stirring. After a desired time (typically 2 h), stirring and introducing oxygen were immediately stopped. The reactor was quickly cooled down to room temperature. Next, the excess oxygen was depressurized slowly. The products were analyzed using a gas chromatograph equipped with an FID detector and a capillary column (DB-624, 30 m × 0.32 mm × 0.25 μm) using ethanol as an internal standard for quantification. Benzyl aldehydes and products were quantified using heptane as an internal standard.

3. Results and discussion

3.1. Textural characterization of $Ce_{1-x}Zr_xO_2$ supports and Au/$Ce_{1-x}Zr_xO_2$ catalysts

Table 1 shows the textural properties of the two series of catalysts prepared by A-$Ce_{1-x}Zr_xO_2$ and B-$Ce_{1-x}Zr_xO_2$. BET data indicates that the catalysts supported on B-$Ce_{1-x}Zr_xO_2$ possess bigger surface area in the range of 77.9-182.2 m^2 g^{-1} than those supported on A-$Ce_{1-x}Zr_xO_2$ (50.1-105.4 m^2 g^{-1}) at the same Ce/Zr molar ratio. The specific surface areas of the two series of catalysts presented almost the same change law, among which Au/A-$Ce_{0.4}Zr_{0.6}O_2$ and Au/B-$Ce_{0.6}Zr_{0.4}O_2$ possessed the highest surface area and the pure oxide ZrO_2 had the lowest surface area. The crystallite size of supports was calculated using Scherrer equation, and the results are shown in Table 1. The mixed oxides A-$Ce_{1-x}Zr_xO_2$ have larger crystallite sizes than B-$Ce_{1-x}Zr_xO_2$ at the same Ce/Zr molar ratio. This characteristic resulted in the larger surface area of series B than that of series of A. For supports B, the crystallite size were small when the Zr content was near to 50 mol %, and the sample B-$Ce_{0.6}Zr_{0.4}O_2$ presented the highest BET surface and smallest crystallite size of 3.5 nm. The lack of a clear trend for the crystallite size for supports A with Zr content could be attributed to the fact that each composition presents a mixture of crystalline structures, which are indicated by the XRD patterns.

The XRD patterns of $Ce_{1-x}Zr_xO_2$ oxides are shown in Figure 1.

The XRD patterns of A-Ce$_{1-x}$Zr$_x$O$_2$ correspond to two phases, the cubic phase of CeO$_2$ and tetragonal phase of ZrO$_2$, indicating that the mixed oxides have their corresponding independent structure. The peak for (220) reflection of CeO$_2$ decreases and the peak for
5 (220) reflection of ZrO$_2$ increases with the increase in Zr content. At the same time, the characteristic diffraction peaks shifted slightly toward high 2θ values, reflecting that the mixed oxides presented little solid solution structure with some Zr doped into the lattice of CeO$_2$. All the B-Ce$_{1-x}$Zr$_x$O$_2$ formed a solid solution,
10 because their XRD patterns are in accordance with the single cubic or tetragonal phase without Zr as a segregated phase.

Compared with pure oxides, the intense lines observed for the mixed oxides of B became broader, which can be contributed to the lattice distortion of cubic phase for CeO$_2$ caused by the
15 incorporation of ZrO$_2$. The main diffraction peaks significantly shift to higher diffraction angles with an increasing amount of Zr content, which could be attributed to the shrinkage of lattice parameter caused by the smaller Zr^{4+} (0.084 nm) cation incorporated into the Ce^{4+} (0.097 nm) lattice.[22] Therefore, the
20 solid solutions B possessed smaller crystallite sizes than supports A and pure oxides as calculated by Scherrer equation (Table 1), which agreed well with the results from HRTEM determination.

Table 1 Characterization of Au/Ce$_{1-x}$Zr$_x$O$_2$ samples

Sample	Au content (wt%) [a]		X value of Ce$_{1-x}$Zr$_x$O$_2$[a]		Lattice		Crystallite size of support [b] (nm)		Surface area [c] (m^2 g^{-1})	
	A	B	A	B	A	B	A	B	A	B
Au/CeO$_2$		1.42		0.0	Cubic			12.6		97
Au/Ce$_{0.8}$Zr$_{0.2}$O$_2$	0.95	1.40	0.18	0.17	-[d]	Cubic	13.8	7.8	80	131
Au/Ce$_{0.6}$Zr$_{0.4}$O$_2$	0.99	1.19	0.41	0.35	-	Cubic	8.4	3.5	85	182
Au/Ce$_{0.4}$Zr$_{0.6}$O$_2$	1.01	1.09	0.60	0.48	-	Tetragonal	11.1	3.9	105	125
Au/Ce$_{0.2}$Zr$_{0.8}$O$_2$	0.94	0.75	0.81	0.75	-	Tetragonal	6.7	5.3	50	78
ZrO$_2$		0.90		1.0	Monoclinic		7.8		50	

[a] Calculated from ICP-OES data. [b] Calculated from value of support plane (111) with Scherrer equation. [c] Determined by N$_2$-BET. [d] Supports A constituted
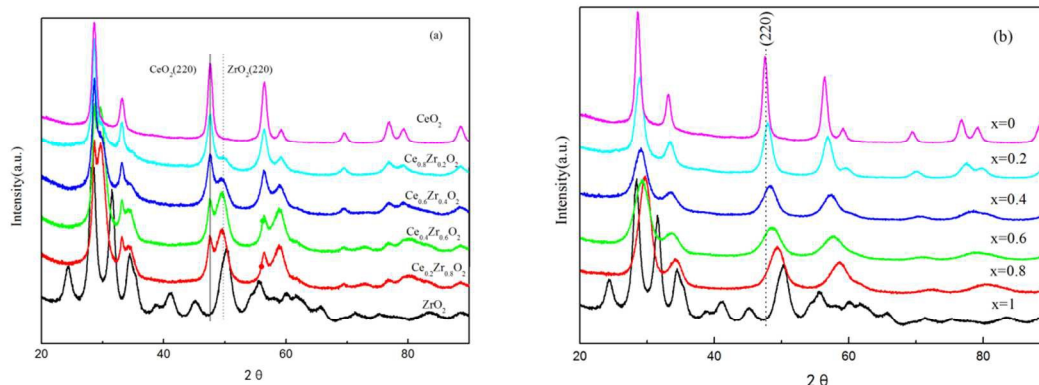25 by cubic CeO$_2$ and tetragonal ZrO$_2$.

Fig. 1 XRD patterns of the supports: (a) A-Ce$_{1-x}$Zr$_x$O$_2$ (x=0-1); (b) B-Ce$_{1-x}$Zr$_x$O$_2$ (x=0-1).

XRD patterns of all catalysts shown in Fig. 2 were almost similar to the patterns for the corresponding support with the
30 same Ce/Zr mole ratio. No obvious Au reflections could be observed for all studied catalysts, indicating the low Au content

or small size of the Au particles, which could not be determined by XRD, and the phases of supports were not transformed after the loading of Au particles.
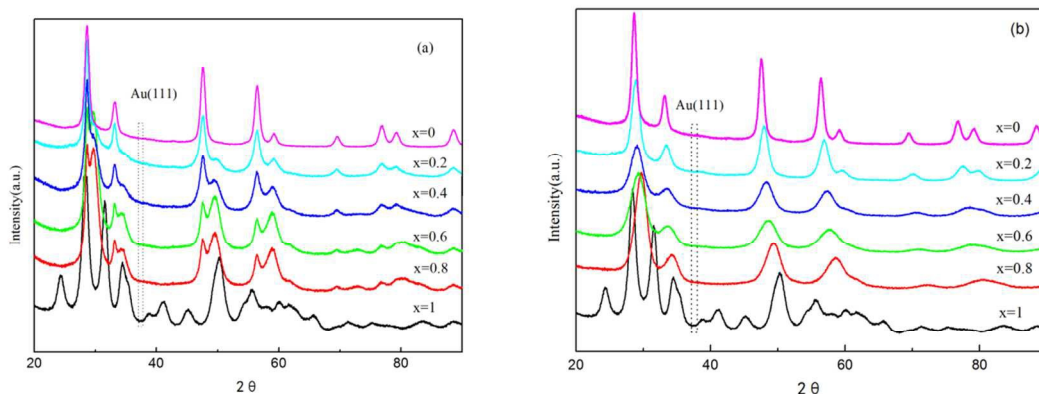
35

Fig. 2 XRD patterns of the catalysts: (a) Au/A-Ce$_{1-x}$Zr$_x$O$_2$ (x=0-1); (b) Au/B-Ce$_{1-x}$Zr$_x$O$_2$ (x=0-1).No Au reflections could be observed and the crystalline phases of Ce$_{1-x}$Zr$_x$O$_2$ supports were not altered after loading Au for all catalysts.
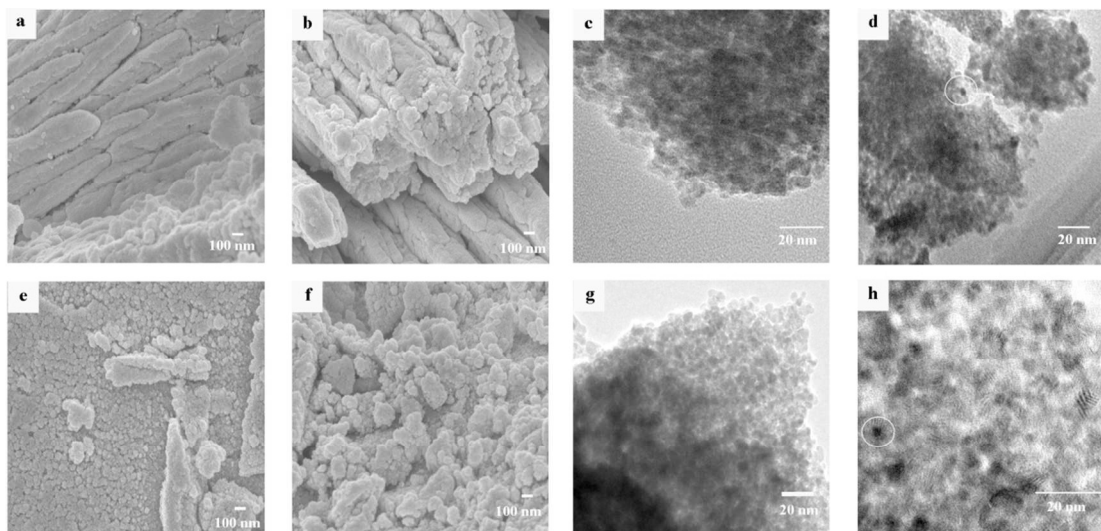

Fig. 3 SEM and TEM images of the supports and the catalysts: (a) A-Ce$_{0.6}$Zr$_{0.4}$O$_2$; (b) Au/ A-Ce$_{0.6}$Zr$_{0.4}$O$_2$; (c) A-Ce$_{0.6}$Zr$_{0.4}$O$_2$; (d) Au/ A-Ce$_{0.6}$Zr$_{0.4}$O$_2$; (e) B-Ce$_{0.6}$Zr$_{0.4}$O$_2$; (f) Au/ B-Ce$_{0.6}$Zr$_{0.4}$O$_2$; (g) B-Ce$_{0.6}$Zr$_{0.4}$O$_2$; (h) Au/ B-Ce$_{0.6}$Zr$_{0.4}$O$_2$. The representative Au particle was indicated by the white circle.
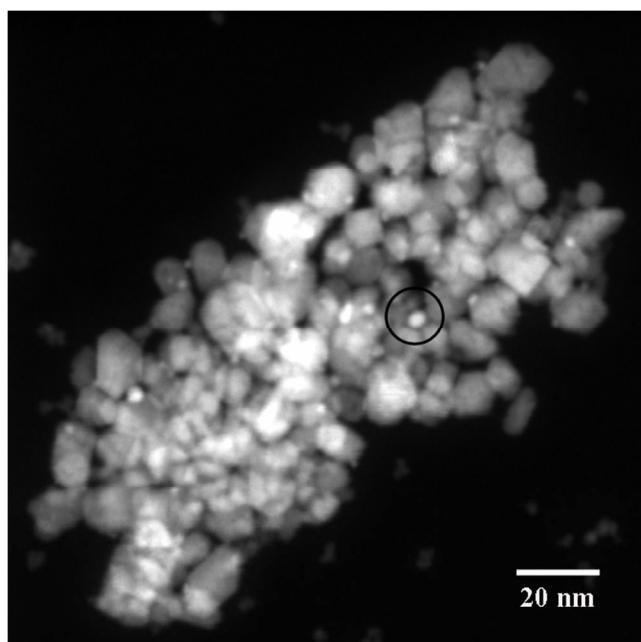

Fig. 4 HAADF-STEM images of Au/B-Ce$_{0.6}$Zr$_{0.4}$O$_2$ catalyst. The representative Au particle was indicated by the black circle.

The morphology of supports and catalysts was viewed by SEM and HRTEM and some representative micrographs are illustrated in Fig. 3, which shows the similarities of the micrographs obtained for two respective series of studied samples. From the SEM micrographs of supports in Fig. 3(a) and (e), the supports of A and B series showed totally different morphologies. The mixed oxides of A were characteristic structure of angular and faced large particles, which is a typical structure for ZrO$_2$, and some smaller spherical grain particles aggregated on the large particles were observed, which is typical structure for CeO$_2$. These finding could be ascribed to the formation of two phases by Ce and Zr respectively almost without solid solution. However, the mixed oxides of B were composed of uniform small grain particles, and more pores in the submicrometer range could be viewed, which are in consistent with BET results for surface area. Comparison with the SEM micrographs of supports, both catalysts A and B present similar morphologies with their supports, indicating that the Au nanoparticles did not change the phase of the supports. The HRTEM pictures show highly dispersed nanoparticles of mixed oxides and Au, and representative Au nanoparticles were indicated by the white circle. All the catalysts possessed similar mean sizes of Au particles of around 3 nm with narrow distributions, and the particle sizes of mixed oxides were around 5-10 nm, which is in agreement with the XRD data.

HAADF-STEM technique (Fig. 4) was used to determine the average Au particle size more accurately, cosidering that some overlapping particles of support could be easily regarded as Au particles. A clear high dispersion of Au and support nanopartilces were observed in the STEM pictures for the sample Au/B-Ce$_{0.6}$Zr$_{0.4}$O$_2$, and the Au particle size distributions were consistant with the HRTEM results. The other catalysts also presented similar Au particle size seen in Fig. S1.

3. 2. Reducibility characterization

H$_2$-TPR is often used as an efficient tool to study the redox property of materials. The supports of series A and B were analyzed by H$_2$-TPR, and the profiles of samples are presented in Figure 5. Pure oxide CeO$_2$ was reduced in two stages, that is, with the profile peaks at 470 ℃ which can contribute to the reduction of easily reducible surface capping oxygen, and peak at 750℃, which could be ascribed to the bulk reduction of CeO$_2$ forming low valence cerium oxides.[27-31] The pure oxide ZrO$_2$ is often considered to be non-reducible at low temperature,[32] and only a small peak was observed around 700 ℃ from the TPR profile of ZrO$_2$. A-Ce$_{1-x}$Zr$_x$O$_2$ (x=0-0.8) showed the similar shape profiles with CeO$_2$ possessing two stages of reduction, while A-

$Ce_{0.2}Zr_{0.8}O_2$ showed no high temperature reduction peak ascribed to the reduction of bulk oxygen. An obvious decrease in the H_2 consumption for supports A with increasing Zr content could be observed from the profiles and the data are shown in Table 2. Those phenomena may have been caused by the fact that the mixed oxides of $A-Ce_{1-x}Zr_xO_2$ formed little structure of solid solution, and thus they mainly presented pure oxides properties as Ce/Zr molar ratio. Even for the Zr-rich sample $A-Ce_{0.2}Zr_{0.8}O_2$, only a small peak around 500 ℃ assigned to the reduction of capping oxygen can be observed because of the thoroughly dispersed CeO_2 on the surface resulting in a total reduction.

Supports B showed totally different change law with supports A. For the Ce-rich solid solutions, all exhibited broader capping oxygen reduction peak than pure CeO_2, which indicated that these solid solutions showed a great promotion of reduction in the bulk oxygen of solid solution. In addition, for all $B-Ce_{1-x}Zr_xO_2$, a shift of maximum of the capping oxygen reduction peak towards higher temperature from 470℃ to 490 ℃ was observed and the starting temperature for H_2 consumption was lower than pure CeO_2. This behavior could be attributed to the phase distortion of mixed oxides, which would alternatively shorten or lengthen the metal-oxygen bonds. Furthermore, the lengthening of the metal-oxygen bond would result in a lower energy barrier for the oxygen migration in the bulk.[31, 32] Consequently, reduction process was no longer confined to the surface but extended deeply into the bulk at lower temperature, resulting in the disappearance of the peak of bulk reduction for Ce-rich solid solutions. Interestingly, the additional shoulder weak peak at 330 ℃ for $B-Ce_{0.8}Zr_{0.2}O_2$ and $B-Ce_{0.6}Zr_{0.4}O_2$ could be ascribed to the reduction of adsorbed surface oxygen species on the free Ce particles,[33, 34] and we postulated that it may be because those two samples possessed bigger surface area. The reduction of $B-Ce_{0.2}Zr_{0.8}O_2$ was similar to that of the two stages reduction of pure CeO_2, which may have resulted from the inhibition of the migration of bulk oxygen to the surface and probable reduction of bulk at high temperature because of the excessive content of ZrO_2 confining the migrating oxygen.
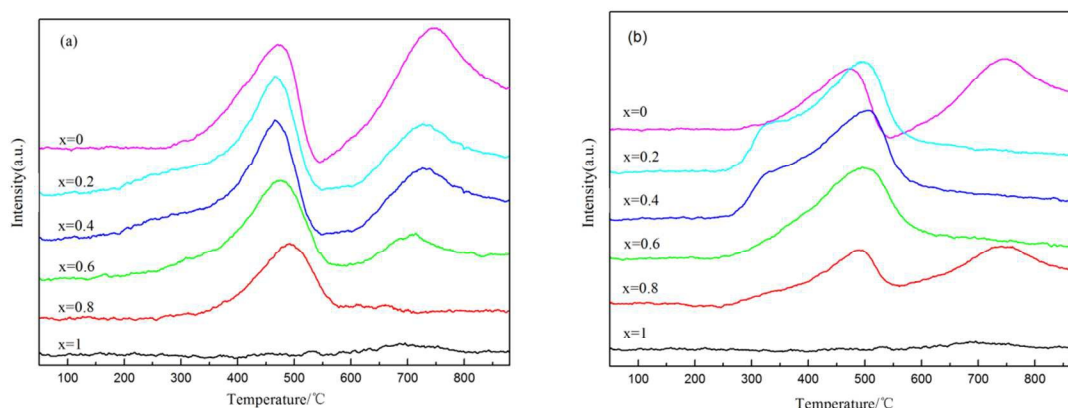

Fig. 5 H_2-TPR profiles of supports: (a) $A-Ce_{1-x}Zr_xO_2$ (x=0-1); (b) $B-Ce_{1-x}Zr_xO_2$ (x=0-1).

The TPR profiles of catalysts are shown in Figure 6 and a significant improvement in Au particles on the reducibility of the oxide supports was observed because of the evident decrease in temperature for reduction. The reduction of all the catalysts occurred in two stage with a higher peak at approximately 100 ℃ . This condition could be ascribed to the reduction in the oxygen species coordinated around finely dispersed Au particles and the Ce surface layers at 400-600 ℃, reflecting the bulk reduction of mixed oxides. Compared with the $Au/A-Ce_{1-x}Zr_xO_2$ with tiny peak of bulk reduction, the $Au/B-Ce_{1-x}Zr_xO_2$ catalysts possessed a higher peak of reduction at 500 °C, which could be assigned to the reduction of capping oxygen, which was similar to the corresponding support. A characteristic decrease in the reduction temperature of catalysts was observed compared with oxide supports. This phenomenon indicates that well-dispersed Au nanoparticles promotes the activation of hydrogen molecule on metallic Au particles and results in the spill-over of dissociated hydrogen from Au nanoparticles to support.[31] Meanwhile, Au could increase the amount of surface oxygen by partial lattice filling of vacant Ce sites with Au.[35] In this case, the presence of Au decreases the strength of the surface Ce-O bonds adjacent to the Au atoms, thus leading to higher surface lattice oxygen mobility.

Table 2 H_2 consumption and surface acidity-basicity for $Ce_xZr_{1-x}O_2$ supports

Sample	Consumption of H_2 (mmol•g^{-1})		Total acidity (mmol NH_3•g^{-1})		Total basicity (mmol CO_2•g^{-1})	
	A	B	A	B	A	B
CeO_2	1.52		0.086		0.65	
$Ce_{0.8}Zr_{0.2}O_2$	1.41	1.81	0.12	0.08	0.68	0.79
$Ce_{0.6}Zr_{0.4}O_2$	1.2	1.85	0.12	0.13	0.88	0.97
$Ce_{0.4}Zr_{0.6}O_2$	1.01	1.84	0.12	0.17	0.75	0.75
$Ce_{0.2}Zr_{0.8}O_2$	0.48	1.59	0.11	0.11	0.81	0.53
ZrO_2	0.09		0.087		0.87	

3. 3. Acid-base property characterization of the support

ZrO_2 dopants in CeO_2 can significantly change the acid-base

properties of the mixed metal oxides.[32, 33] The loading of Au particles changes the acid-base properties of support slightly. Hence, we just use the acid-base properties of support instead of catalyst to research the effects of support in the following discussion. The acid-base properties of all oxides were revealed by NH_3-TPD and CO_2-TPD analysis. The results are shown in Figs. 7 and 8. Data are summarized in Table 2.

The mixed oxides prepared by method A have similar profiles and presented almost similar total acidity amount around 0.12 mmol NH_3 per gram catalysts. Meanwhile, the mixed oxides of supports A had more strong acidic sites, which were assigned to the shoulder peak around 550 °C, with increasing of Zr content. However, the solid solutions presented different acidic site concentrations and acidity distributions, which had two big peaks presenting the weak and strong acidic sites respectively. The

amounts of weak acidic sites for $B-Ce_{1-x}Zr_xO_2$ ranged from 0.075 mmol to 0.090 mmol NH_3 per gram catalysts, which is higher than the $A-Ce_{1-x}Zr_xO_2$. The support $B-Ce_{0.4}Zr_{0.6}O_2$ with a broad peak around 450 °C possessed the highest amount of strong acidic sites, which was twice that of other mixed oxides. The sample $B-Ce_{0.6}Zr_{0.4}O_2$ presented weakest acidic sites with a broad peak around 200 °C. The phenomenon may be attributed to the weak acidic sites connection of the surface area, with $B-Ce_{0.6}Zr_{0.4}O_2$ as having the largest surface area in all solid solutions. It was reported that[37] the incorporation of increasing quantities of Zr in the Ce lattice leads to a marked increase in the total and strong acidity, while our catalyst $B-Ce_{0.4}Zr_{0.6}O_2$ possessed highest amount of acidic sites and strong acidity. The present results may be not comparable between our results and literature with using different synthesizing methods.
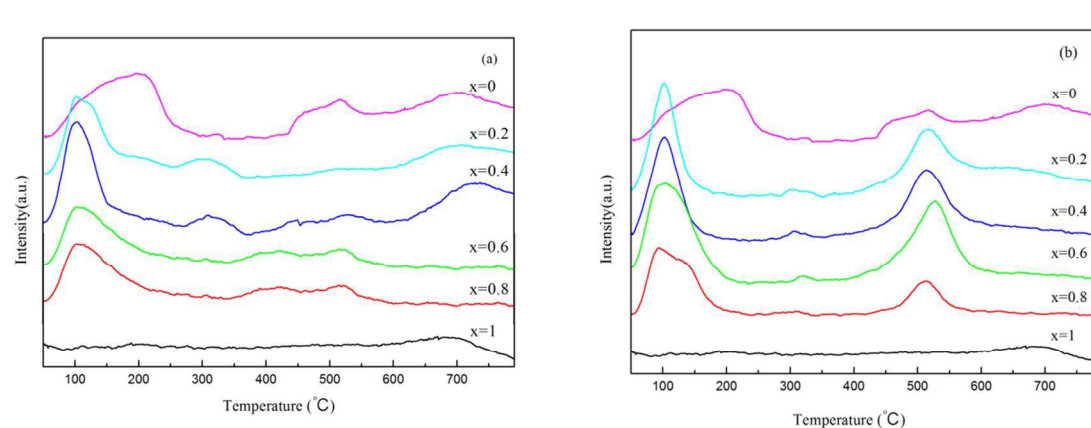

Fig. 6 H_2-TPR profiles of catalysts: (a) $Au/A-Ce_{1-x}Zr_xO_2$ (x=0-1); (b) $Au/B-Ce_{1-x}Zr_xO_2$ (x=0-1).

The base properties for all oxides are shown in Fig. 8. The surface base concentrations of $A-Ce_{1-x}Zr_xO_2$ ranged from 0.68 mmol to 0.88 mmol CO_2 per gram support. The surface base concentrations of $B-Ce_{1-x}Zr_xO_2$ ranged from 0.53 mmol to 0.97 mmol CO_2 per gram support. Similar to the change law of acidity properties for $A-Ce_{1-x}Zr_xO_2$ and $B-Ce_{1-x}Zr_xO_2$, the base concentrations and distribution of the basic sites for $A-Ce_{1-x}Zr_xO_2$

were presented as preparing by mechanical mixing according to fixed Ce/Zr content. The solid solutions of $B-Ce_{1-x}Zr_xO_2$ had more basic sites and higher concentrations than pure oxides. The solid solutions $B-Ce_{1-x}Zr_xO_2$ had more kinds of basic sites, all of which had a broad strong base peak with $B-Ce_{0.6}Zr_{0.4}O_2$ having the highest amount of basic sites.
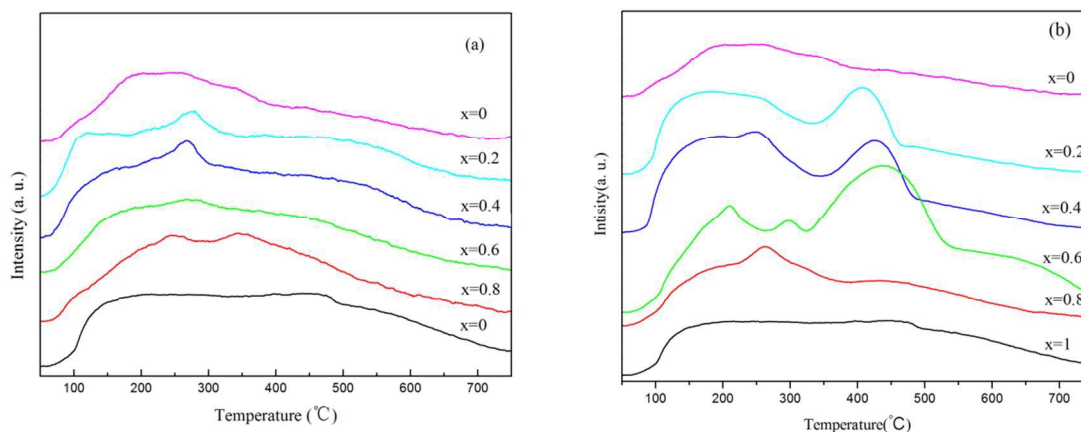

Fig. 7 NH_3-TPD profiles of $Ce_xZr_{1-x}O_2$ supports: (a) $A-Ce_{1-x}Zr_xO_2$ (x=0-1); (b) $B-Ce_{1-x}Zr_xO_2$ (x=0-1).

Comparative results of the NH_3-TPD and CO_2-TPD data showed that all supports possess both acidic and basic sites, with

a more pronounced basic character in terms of concentration of basic sites and strong adsorption sites. Meanwhile, most solid

solutions present more acidic and basic sites in terms of concentration and kinds of different sites than the series of support A, which possesses more acidic and basic sites than pure oxides caused by the formed partial solid solution structure. A thorough review of the literature suggests that oxygen mobility is favored in Ce-Zr solid solutions because of the substitution of Ce^{4+} by the smaller Zr^{4+} cation. This phenomenon causes shrinkage of the CeO_2 fluorite-type lattice, which generates

surface oxygen anions as basic sites in the catalyst Thus, the substitution of Ce^{4+} cation with the smaller Zr^{4+} cation distorts the cubic structure of CeO_2, and results in the solid solutions supports B to exhibit stronger acidity/basicity as well as higher amount of oxygen available. At the same time, the size of the Au particles in all the catalysts differed slightly, which facilitated the understanding of the intrinsic support effects on these Au catalysts in aldehyde oxidative esterification.
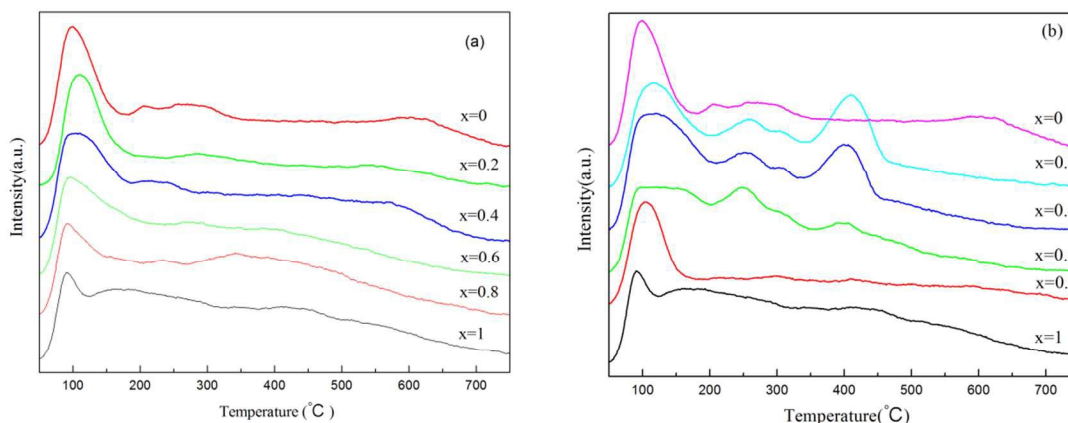

Fig. 8 CO_2-TPD profiles of $Ce_xZr_{1-x}O_2$ supports: (a) A-$Ce_{1-x}Zr_xO_2$ (x=0-1); (b) B-$Ce_{1-x}Zr_xO_2$ (x=0-1).

3.4. Catalytic performance on oxidative esterification of aldehyde

Catalytic activities were evaluated for the oxidative esterification

of a number of aldehydes. First, the catalyst screening was obtained by oxidative esterification of isobutyraldehyde.

3.4.1. Catalyst screening and the effects of support

Table 3 Catalytic performance for oxidative esterification of isobutyraldehyde with methanol to form methyl isobutyrate[a]

Sample		Conversion/%[b]	Selectivity/%[b]		
			Methyl isobutyrate	Dimers of ISB	Others[c]
B-$Ce_{0.6}Zr_{0.4}O_2$		3.42	0	96.7	1.52
Au/CeO_2		96.9	81.0	2.2	13.7
Au/$Ce_{0.8}Zr_{0.2}O_2$	A	61.0	87.5	2.1	10.1
	B	96.4	80.9	3.8	14.1
Au/$Ce_{0.6}Zr_{0.4}O_2$	A	69.9	72.6	10.3	18.2
	B	98.0	83.8	4.1	10.2
Au/$Ce_{0.4}Zr_{0.6}O_2$	A	32.0	43.1	35.2	19.1
	B	97.7	82.2	3.8	13.6
Au/$Ce_{0.2}Zr_{0.8}O_2$	A	13.5	82.6	2.1	13.2
	B	66.5	68.4	2.3	27.1
Au/ZrO_2		15.8	94.5	2.2	1.6

[a] Reaction conditions: catalyst :0.50g; K_2CO_3:0.10 g; ISB=0.05 mol; methanol=40 mL; O_2=15 ml/min; P=0.3 MPa；at 80 °C for 2 h. [b] Determined by GC analysis. [c] others include dimers of the isobutyraldehyde, acetal, CO_2, and some unknown products.

Two series of Au supported on different Ce/Zr oxides and pure oxides were tested for the oxidative esterification of isobutyraldehyde (ISB), and the catalytic results are shown in Table 3. The support Ce-Zr oxides or pure oxides without loading of Au nanoparticles presented no activity for oxidative esterification. The reaction data is shown in table 3 using representative B-$Ce_{0.4}Zr_{0.6}O_2$ as catalyst. Only little of ISB was mainly transformed into dimers of itself and no methyl isobutyrate was detected. Compared with Au/B-$Ce_{1-x}Zr_xO_2$ (x=0.2-0.8) catalysts, the series of Au/A-$Ce_{1-x}Zr_xO_2$ (x=0.2-0.8) catalysts preformed badly with lower conversion by 30%. With

the increase in Zr content of the mixed oxides of A, the conversion first slightly increased a little from 61.0% to 69.9%, then decreased sharply to 13.5%; the selectivity dropped first from 87.5% to 43.1%, then increased to 82.2%. The main by-products during the direct oxidative esterification of the ISB are dimers of itself, acetal, isobutyric acid and CO_2, which mainly produced by the over oxidation of isobutyraldehyde. The series of Au supported on mixed oxides of B all showed good performance on the esterification of ISB with the yield of methyl isobutyrate above 78%, except of Au/B-$Ce_{0.2}Zr_{0.8}O_2$ with low yield. The highest yield of 82.1% for methyl isobutyrate in ISB oxidative

esterification was obtained using the $Au/B-Ce_{0.6}Zr_{0.4}O_2$ catalyst. To determine the essential reason for the different activities of all mixed oxides, the relation of the yield of methyl isobutyrate and physical-chemical properties of supports were investigated in detail. The effect of reducibility, acidity and basicity of mixed oxides for the catalytic activity is shown in Figure 9. For both A and B series, the sequence of increasing the H_2 consumption clearly follows the sequence of increasing activity of the catalyst for corresponding support on the whole. Thus, the observed correlations indicate that the higher H_2 consumption of $Au/A-Ce_{0.8}Zr_{0.2}O_2$ and $Au/B-Ce_{0.6}Zr_{0.4}O_2$ might be responsible for the

higher yield of ester for each series studied catalysts, while the catalysts prepared by supports with high content of Zr, particular for pure oxide ZrO_2, presented lower activity due to their weaker reducibility. These findings indicate that the reducibility of the support plays an important role in the performance of studied catalysts in oxidative esterification of ISB. However, high activity with high consumption of H_2 is not inevitable, considering that catalysts B with almost the same reducibility possessed. Therefore, determining other factors of the support that impact the activity is necessary.
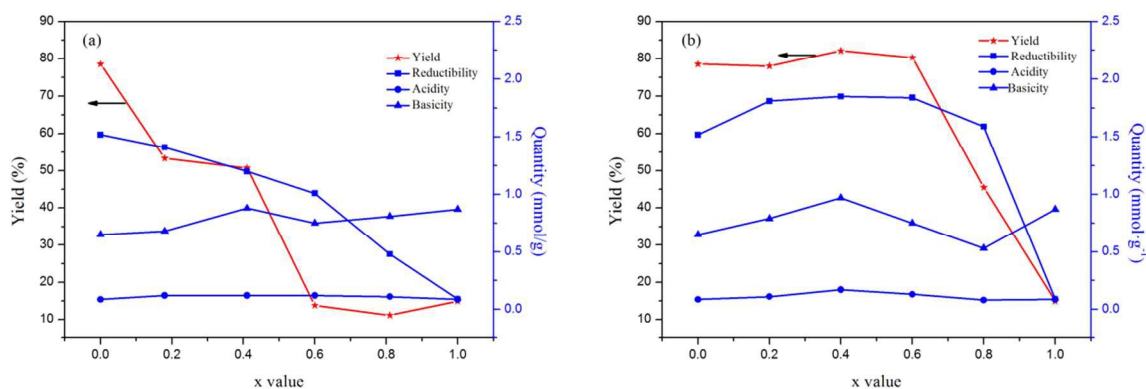

Fig. 9 Effects of reducibility, acidity and basicity of supports on the catalytic activity. (a) $A-Ce_{1-x}Zr_xO_2$ (x=0-1); (b) $B-Ce_{1-x}Zr_xO_2$ (x=0-1)

The relation between yield and acid-base properties of support is also shown in Fig. 9 (b) for series B. Evident correlation was found between the acid-base properties of the support and yield of ester. The catalyst $Au/B-Ce_{0.4}Zr_{0.6}O_2$ with most acidic and basic sites illustrated the highest activity, while the catalyst $Au/B-Ce_{0.6}Zr_{0.4}O_2$ with small amount of acidic and basic sites showed

quite low activity. The sample Au/ZrO_2 possessing high acidic sites presented worst activity assigned to the unreducible of ZrO_2. These results allowed us to conclude that the acidity and basicity of support also play an important role on oxidative esterification of aldehydes in the proposed catalytic system.
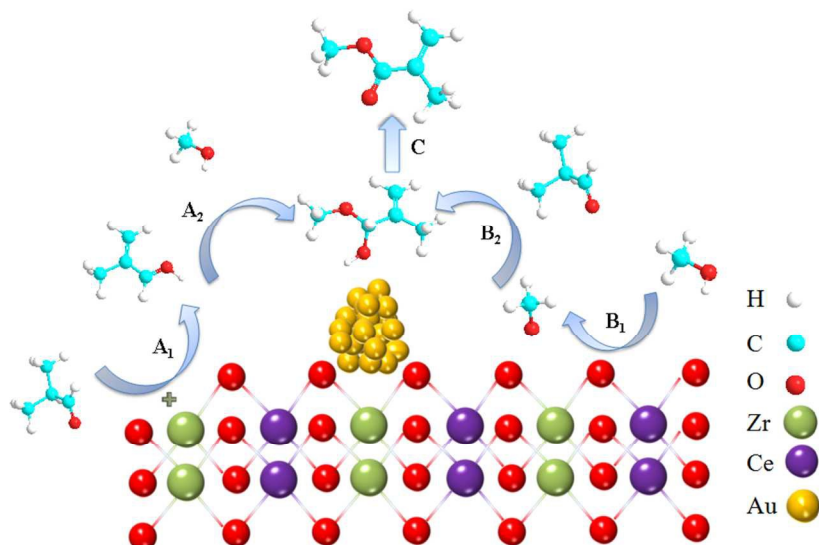

Fig. 10 Plausible reaction mechanism for oxidative esterification of aldehydes on Ce-Zr solid solution supported Au nanoparticles

The reaction mechanism for the oxidative esterification of aldehydes with alcohols over the Pd- and Au-based catalysts was recently investigated in detail[8, 10, 36-38]. Generally, the reaction for the direct oxidation oxidative esterification of aldehydes to esters involves two steps. Initially, hemiacetal is formed by

condensation reaction between aldehyde and alcohol. The formation of hemiacetal is easily effected by the acidity/basicity of support. Zheng et al.[8] and Wang et al.[11] found that stronger acidity/basicity of support, respectively, was in favor of forming hemiacetal, which could lead to higher selectivity of esters. Then,
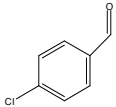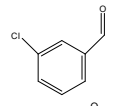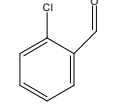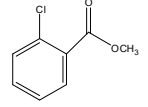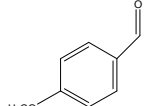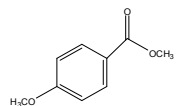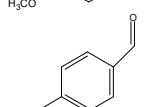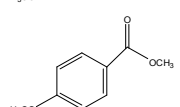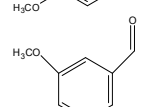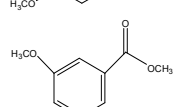
the ester is produced by the abstraction of H from hemiacetal. Thus, considering the correlation of reducibility and activity, we speculate the reaction mechanism for oxidative esterification of isobutyraldehyde on solid solution supported Au nanoparticles, which is shown in Fig. 10. First, the formation of hemiacetal could be enhanced through two routes by acidic and basic sites respectively. The acidic sites could facilitate the aldehyde into oxonium ion, while the basic sites can activate methanol into methoxy and sequentially, both the oxonium and methoxy have a beneficial effect to form the intermediate hemiacetal by ease of nucleophilic reaction as shown in step A and step B. It is noteworthy that the hemiacetal might mainly formed by route B due to all the catalysts possessing more basic sites than acidic sites according the results of NH_3-TPD and CO_2-TPD. Then, the ester is formed by the abstraction of β-H from hemiacetal. The atomic oxygen plays a very important role during the whole pathway, which is beneficial to the abstraction of H from methanol to methoxy and the β-H elimination of hemiacetal to ester. The active atomic oxygen can be produced by the direct activation of molecular oxygen on the supported small enough Au nanoparticles and be enhanced by the spillover from the lattice oxygen of the oxides supports due to the interaction between Au nanoparticles and the support[39]. That is why the bare support presented no activity for the formation of ester and the samples with larger amounts of H_2 consumption presented higher activity. For the catalysts A supported on mixed oxides, the effect of acid-base properties did not show prominent role due to the low consumption of H_2 considering the step C as the rate determining step. Therefore, for all the catalysts prepared by mixed oxides and pure oxides, higher reducibility and basicity of the support are in favor of ester formation.

3.4.2. Optimization of substrates scope and recycling uses of Au/B-Ce$_{0.6}$Zr$_{0.4}$O$_2$ catalyst

To examine the effect of the substrate structure on reactivity, the reactions of a range of benzylic aldehyde were examined using the Au catalyst supported on solid solution B-Ce$_{0.6}$Zr$_{0.4}$O$_2$. It is because that B-Ce$_{0.6}$Zr$_{0.4}$O$_2$ has been found to be the most active at the same preparation condition. The results are summarized in Table 4. To obtain a high yield of the product, the reaction time is not the major factor for consideration. Benzylic aldehyde with electron-donating and electron-withdrawing groups gave excellent yields of products (Table 4, entries 1–7). Similar to para-and meta-substituted substrates, the sterically more hindered ortho-substituted aldehyde also provided excellent results under the same reaction conditions.

Table 4 Au-catalyzed oxidative esterification of benzylic aldehyde with methanol[a]

Entry	Substrate	Product	Reaction time/h	Base/mol%	Conversion/%	Selectivity/%
1			2	5	98.0	89.5
2			12	3	91.2	98.5
3			12	3	94.3	95.6
4			12	1	63.7	94.2
5			12	3	82.9	93.6
6			12	3	99.5	99.1

[a] Footnote text.

Stability is a key requirement of an effective catalyst for its practical application, besides the selectivity of methyl benzoate. Thus, the recycling use of the Au/B-Ce$_{0.6}$Zr$_{0.4}$O$_2$ catalyst for the oxidative esterification of benzaldehyde with methanol was conducted. The catalyst was recovered by removing the supernatant after the reaction mixture was left undisturbed for a time, and washed with methanol, followed by supernatant removal. The procedure was repeated twice, and then the catalyst was reused. Fig. 10 shows that the benzaldehyde conversion decreased only slightly in the initial 7 recycles, and then kept almost unchanged in the 8th recycle. Meanwhile, methyl benzoate was a constant selectivity of as high as 99%. After 8 recycles, the benzaldehyde conversion and the methyl benzoate yield could still be sustained at >95%. This phenomenon indicates that the Au/B-Ce$_{0.6}$Zr$_{0.4}$O$_2$ catalyst is stable during the recycling uses for the conversion of benzaldehyde with methanol in the presence of O_2.
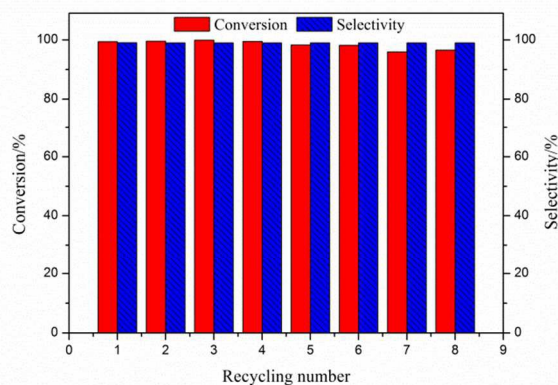
Fig. 11 Catalytic performance of the recycled Au/Ce$_{0.6}$Zr$_{0.4}$O$_2$ for the oxidative esterification of benzaldehyde. Reaction conditions: Catalyst 0.5g, benzaldehyde 0.04mol, K$_2$CO$_3$ 0.15 g, methanol 40 mL, P(O$_2$)=0.3 MPa, T=353 K, t=2 h.

4. Conclusions

Two series of Ce$_{1-x}$Zr$_x$O$_2$ (x = 0, 0.2, 0.4, 0.6, 0.8, and 1) oxides were prepared using different Ce precursors by hydrothermal method. Highly uniform and nanosized, Ce/Zr solid solutions were obtained using ammonium ceric nitrate as precursors, while mixed oxides were obtained using cerium nitrate. Given the smaller Zr^{4+} incorporated into the CeO$_2$ structure, the solid solutions B-Ce$_{1-x}$Zr$_x$O$_2$ presented smaller crystallite size, as well as stronger acidity/basicity and reducibility, than the mixed oxides of A-Ce$_{1-x}$Zr$_x$O$_2$ at the same Ce/Zr molar ratio. In addition, the Au catalysts on supports B showed better performance than those on supports A for oxidative esterification of Isobutyraldehyde at the same Ce/Zr molar ratio. The highest activity with the conversion 98.0% and selectivity 83.8 for methyl isobutyrate can be observed using Au/B-Ce$_{0.4}$Zr$_{0.6}$O$_2$ as catalyst, which presents the stronger reducibility and highest amount of acidic sites. A correlation between catalytic activity and reducibility of the support was observed. Higher reducibility of support is remarkably favorable for oxidative esterification reaction. The support with high reducibility could produce more active atomic oxygen by interaction between Au nanoparticles and support through lattice oxygen spillover, which could improve the activity of catalyst by activation of methanol to methoxy and facilitating the β-H elimination of hemiacetal. For supports B which possessed almost the same reducibility, the acidity and basicity also play an important role on facilitating oxidative esterification of aldehyde, which could improve the formation of intermediate hemiacetal and thus enhance the formation of ester. The screening catalyst was applicable to the oxidative esterification of different benzyl aldehydes with high yields above 90%, which commonly have lower conversion than aliphatic aldehyde. The catalyst could be reused after a simple separation for eight times keeping high selectivity above 99% with only a slight decrease in conversion from 99% to 96%.

Notes and references

^{a} *Beijing Key Laboratory of Ionic Liquids Clean Process, State Key Laboratory of Multiphase Complex System, Institute of Process Engineering, Chinese Academy of Sciences, Beijing 100190, China Fax: XX XXXX XXXX; Tel: 86-10-82544875; E-mail: sjzhang@ipe.ac.cn*
^{b} *College of Chemical and Engineering, University of Chinese Academy of Sciences, Beijing 100049, China*
†*Electronic Supplementary Information (ESI) available: [details of any supplementary information available should be included here]. See DOI: 10.1039/b000000x/*

References

1. Otera, J.Esterification: Methods, Reaction and Applications; WileyVCH: Weinheim, Germany, 2003.
2. R. C. Larock, Comprehensive Organic Transformations; VCH:New York,1989.
3. T. Ogawa and M. Matsui, *J. Am. Chem. Soc.*, 1976, **98**, 1629.
4. T. Suzuki, K. Morita, M. Tsuchida and K. Hiroi, *Org. Lett.*, 2002, **4**, 2361.
5. T. Hayashi, T. Inagaki, N. Itayama and H. Baba, *Catal. Today*, 2006, **117**, 210.
6. C. Marsden, E. Taarning, D. Hansen, L. Johansen, S. K. Klitgaard, K. Egeblad and C. H. Christensen, *Green Chem.*, 2008, **10**, 168.
7. M. Haruta, N. Yamada, T. Kobayashi and S. Iijima, *J. Catal.*, 1989, **115**, 301.
8. F.-Z. Su, J. Ni, H. Sun, Y. Cao, H.-Y. He and K.-N. Fan, *Chem. Eur. J.*, 2008, **14**, 7131.
9. P. Fristrup, L. B. Johansen and C. H. Christensen, *Chem. Commun.*, 2008, 2750.
10. K. Suzuki, T. Yamaguchi, K. Matsushita, C. Iitsuka, J. Miura, T. Akaogi and H. Ishida, *ACS Catal.*, 2013, **3**, 1845.
11. X.-Z. Wan, W.-P. Deng, Q.-H. Zhang and Y. Wang, *Catal. Today*, 2014, **233**, 147.
12. N. Lopez, T. V. W. Janssens, B. S. Clausen, Y. Xu, M. Mavrikakis, T. Bligaard and J. K. Nørskov, *J. Catal.*, 2004, **223**, 232
13. T. V. Choudhary and D. W. Goodman, *Appl. Catal., A*, 2005, **291**, 32
14. M. Haruta, *Gold Bull*, 2004, **37**, 27.
15. X. Feng, X. Duan, G. Qian, X. Zhou, D. Chen, and W. Yuan, *J. Catal*, 2014, **317**, 99–104.
16. M. Murdoch, G. I. N. Waterhouse, M. A. Nadeem, J. B. Metson, M. A. Keane, R. F. Howe, J. Llorca and H. Idriss, *Nature Chem.*,2011, **3**, 489–492.
17. S. Carrettin, P. Concepción, A. Corma, J. M. L. Nieto and V. F. Puntes, *Angew. Chem., Int. Ed.*, 2004, **43**, 2538.
18. T. V. W. Janssens, A. Carlsson, A. Puig-Molina and B. S. Clausen, *J. Catal.*, 2006, **240**, 108.
19. Z. Ma, C. Liang, S.H. Overbury and S. Dai, *J. Catal.*, 2007, **252**, 119.
20. A.S.K. Hashmi and G.J. Hutchings, *Angew. Chem., Int. Ed.*, 2006, **45**, 7896.
21. J. Saavedra, H. A. Doan, C. J. Pursell, L. C. Grabow, and B. D. Chandler, *Science*, 2014, **349**, 1599.
22. M. Daturi, C. Binet, J.C. Lavalley and G. Blanchard, *Surf. Interface Anal.*, 2000, **30**, 273.
23. V. Shapovalov and H. Metiu, *J. Catal.*, 2007, **245**, 205.
24. C. M. Kalamaras, D. D. Dionysiou, and A. M. Efstathiou, *ACS Catal.*, 2012, **2**, 2729.
25. R. Si, Y.-W. Zhang, S.-J. Li, B.-X. Lin and C.-H. Yan, *J. Phys. Chem. B*, 2004, **108**, 12481.
26. S.-P. Wang, T.-Y. Zhang, X.-Y. Wang, S.-M. Zhang, S.-R. Wang, W.-P. Huang and S.-H. Wu, *J. Mol. Catal. A: Chem.*, 2007, **272**, 45.

27. A. Sepúlveda-Escribano, F. Coloma and F. Rodriguez-Reinoso, *J. Catal.*, 1998, **178**, 649.
28. F. Giordano, A. Trovarelli, C. de Leitenburg and M. Giona, *J. Catal.*, 2000, **193**, 273.
5 29. P. Concepción, A. Corma, J. Silvestre-Albero, V. Franco and J.Y. Chane-Ching, *J. Am. Chem. Soc.*, 2004, **126**, 5523.
30. L. Ilieva, J. W. Sobczak, J. M. Manzoli, B. L. Su and D. Andreeva, *Appl. Catal., A*, 2005, **291**, 85.
31. I. Dobrosz-Gómez, I. Kocemba and J. M. Rynkowski, *Appl. Catal., B*, 2008, **83**, 240.
10
32. I. Dobrosz-Gómez, I. Kocemba and J. M. Rynkowski, *Catal. Lett.*, 2009, **128**, 297.
33. N. Liu, Z. Yuan, S. Wang, C. Zhang, S. Wang and D. Li, *Int. J. Hydrogen Energy*, 2008, **33**, 164.
15 34. J.-a. Wang, L.-f. Chen and C.-l. Li, *J. Mol. Catal. A: Chem.*, 1999, **139**, 318.
35. Q. Fu, H. Saltsburg and M. Flytzani-Stephanopoulos, *Science*, 2003, **301**, 935.
36. Y. Diao, R. Yan, S. Zhang, P. Yang, Z. Li, L. Wang and H. Dong, *J. Mol. Catal. A: Chem.*, 2009, **303**, 35.
20
37. O. Casanova, S. Iborra and A. Corma, *J. Catal.*, 2009, **265**, 109.
38. B. Xu, X. Liu, J. Haubrich and C. M. Friend, *Nature Chem.*, 2010, **2**, 61.
39. Y. Wei, J. Liu, Z. Zhao, A. Jun and G. Jiang, *J. Catal.*, 2012, **287**, 13.
25

Catalysis Science & Technology Accepted Manuscript
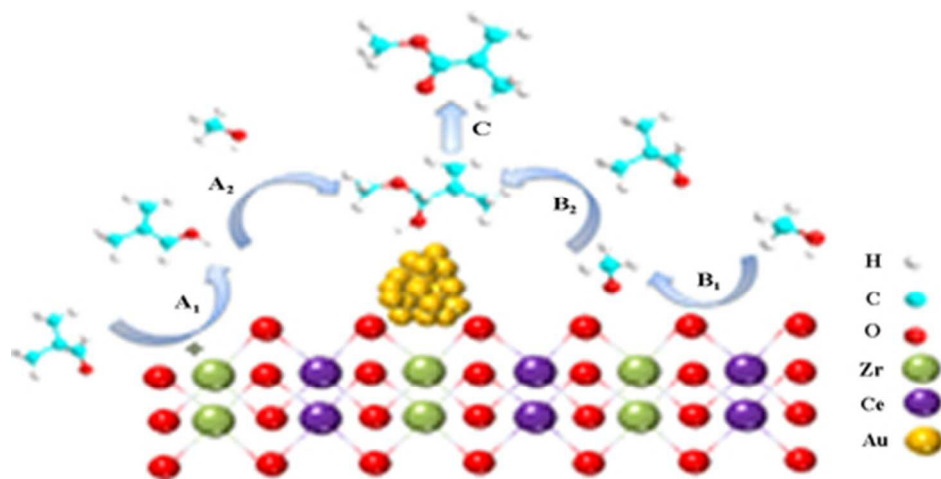
Au nanoparticles supported on Ce0.6Zr0.4O2 solid solution with high reducibility and basicity is efficient catalyst for oxidative esterification.
39x19mm (300 x 300 DPI)